Title
Thermoelectric Coolers and Power Generators Using Self-assembled Ge Quantum Dot Superlattices

Author
Liu, Jianlin

Publication Date
2004-09-01

Fundamental Science of Energy 005

"Thermoelectric Coolers and Power Generators Using Self-assembled Ge Quantum Dot Superlattices"

Jianlin Liu

September 2004

This paper is part of the University of California Energy Institute's (UCEI) Energy Policy and Economics Working Paper Series. UCEI is a multi-campus research unit of the University of California located on the Berkeley campus.

UC Energy Institute
2547 Channing Way, # 5180
Berkeley, California 94720-5180
www.ucei.berkeley.edu

1. Technical report

The proposed goal of this proposal is to explore the Ge quantum dot superlattices for thermoelectric device applications. Over 1-year period, we have worked on this project extensively and achieved the following research results:

a) Mobility of Ge quantum dot superlattice

Quantum dots and different types of quantum dot arrays continue to attract significant attention of the physics and device research communities [for review see K. L. Wang and A. A. Balandin, Properties and Applications of Quantum Dots, in *Optics of Nanostructured Materials*, edited by V. Markel and T. George (Wiley and Sons, New York, 2001) p.515-551.]. Quantum dot superlattices (QDS) have been proposed for thermoelectric applications in this proposal. For this application, it is crucial to maintain relatively high carrier mobility or product of the mobility and carrier concentration. Good carrier mobility and electric conductivity are important for thermoelectric materials where the figure of merit Z at given temperature T is defined as $ZT=\alpha^2\sigma T/K$ (α is Seebeck coefficient, σ is electrical conductivity, K is thermal conductivity). Carrier transport in quantum dot arrays can manifest both hopping transport and conduction band transport features [H. Z. Song, K. Akahane, S. Lan, H. Z. Xu, Y. Okada, and M. Kawabe, *Phys. Rev. B*, **64**, 085303 (2001).]. The hopping transport regime is characterized by much lower mobility values than the band conduction transport, and by different temperature dependence. What transport regime would prevail depends on the structural and morphological properties of QDS. Despite its importance for practical applications there have been little work done on carrier transport in QDS [A. I. Yakimov, C. J. Adkins, R. Boucher, A. V. Dvurechenskii, A. I. Nikiforov, O. P. Pchelyakov, and G. Biskupski, *Phys. Rev. B*, **59**, 12598 (1999).].

In this research, we accomplished measurements of Hall mobility in a set of Ge_xSi_{1-x}/Si QDS grown by molecular beam epitaxy (MBE). We have used two batches of QDS samples (both doped and undoped) fabricated by two different research groups. The undoped samples JL264 and JL265 with typical Ge content in the dots of 50% have been

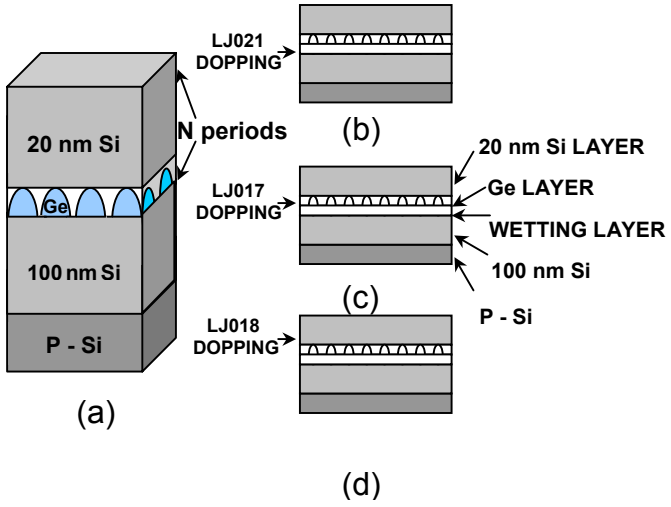

Fig.1 Schematic of sample structure (a), and location of the δ-doping (b).

grown in a Perkin Elmer MBE system. The doped samples LJ017, LJ018 and LJ021 with Si content in the dots less than 27% have been grown in a Riber EVA32 at UCLA. All investigated QDS with either 5 or 20 layers of quantum dots have been grown on p-type Si wafers (see Fig. 1 (a)). There are three different positions for δ-doping layer in the doped QDS (Fig. 1 (b-d)). Although Hall mobility μ_H cannot be easily translated to the electron (hole) drift mobility μ_e (μ_h), unless the sample has only one type of carriers, it represents a measure of the overall mobility of both electrons and holes in given sample.

The Ge/Si QDS samples used in this study were fabricated using a solid-source MBE system. P-type (100) Si with a resistivity of 8-10 Ω cm was used as a substrate and cleaned using a standard Shiraki clearing method followed by *in situ* thermal cleaning at 930°C for 15 min. The substrate temperature has been maintained at 550 °C during the epitaxial growth. The nominal growth rates were 1 Å/s and 0.05 Å/s for Si and Ge, respectively. Four types of samples have been grown. The first type is undoped and the other three types are boron δ-doped in wetting layer, 6 Å Ge dots layer and Si cap layer, respectively (see Fig. 1 (b-d)). Boron doping is achieved by sublimation of boron from a Knudsen cell. The samples consist of a 100 nm undoped Si buffer layer, 5 or 20 periods of Ge quantum dots separated by 20 nm-thick Si spacer layer and 50 nm-thick cap layer on the top (Fig. 1 (a)). The doping density in the Si capping layer was about 5×10^{18} cm^{-3}.

Thermally diffused contacts made of aluminum were formed on top of the superlattices to carry out Hall measurements. Extended annealing time has been chosen to make sure that the contact is formed for all layers of quantum dots. The voltage was applied across the gap between the pairs of two electrodes, so that current flows parallel to the quantum dot layers. The Hall mobility was measured using EGK HEM-2000 system at the room temperature and 77 K. The measurements were conducted in a standard four-terminal scheme to ensure the accuracy. The data points were taken at the magnetic field of 0.37 T. Before measuring mobility in QDS we have tested the setup and experimental procedure on several reference samples consisted of conventional Si/Ge quantum well superlattices.

In Fig. 2 (a-b) we present Hall mobility in p-type doped Ge/Si quantum dot superlattices at room temperature and 77 K. The Hall mobility μ_H is shown as a function of input current I_{inp} to demonstrate its weak dependence on I_{inp}. The Hall mobility μ_H is defined as the product of the Hall coefficient R_H and the electric conductivity σ

$$\mu_H = \left| R_H \sigma \right|. \qquad (1)$$

Here $R_H = \dfrac{p - nb^2}{e(p + nb)^2}$, and $b = \mu_e / \mu_h$ is the ratio of the electron μ_e and hole μ_h drift mobilities, n (p) is the electron (hole) density, and e is the charge of an electron. As one can see from Eq. (1), the Hall mobility should be clearly distinguished from the drift mobilities. The Hall mobility can be more readily correlated with the electron or hole mobilities for the heavily doped samples where $n>>p$ (or $p>>n$). In the general case, the Hall mobility is related to the drift mobility (one type of carriers) through the expression $\mu_H = <<\tau^2>>/<<\tau>>^2 \mu_{drift}$ [J. Singh, *Physics of Semiconductors and Their Heterostructures* (McGraw-Hill, Inc., 1993).]. Here τ is the scattering time, the symbol $<<>>$ denotes averaging for the relaxation time defined as $<<\tau>> = <E\tau>/<E>$, where E is the energy of the carrier and symbol $<>$ denotes standard ensemble average. The measured values of the Hall coefficient were positive indicating the overall p-type

conduction. Table I summarizes the average measured values of the Hall mobility for the undoped and doped quantum dot superlattices.

For comparison, the room temperature electron (hole) drift mobility in bulk Si and Ge are μ_e = 1500 $cm^2V^{-1}s^{-1}$ (μ_p = 450 $cm^2V^{-1}s^{-1}$) and μ_e = 3900 $cm^2V^{-1}s^{-1}$ (μ_p = 1900 $cm^2V^{-1}s^{-1}$), respectively. Electron (hole) drift mobility at 77K can be estimated from the equation $\mu = \mu_0 \left(\frac{T}{T_0} \right)^{-3/2}$, where T_0 =300 K and μ_o is the drift mobility at T=300 K [S. M. Sze, *Semiconductor Devices: Physics and Technology* (Wiley, New York, 1985).]. Thus, at 77 K one gets $\mu_e = 3.0 \times 10^4$ $cm^2V^{-1}s^{-1}$, $\mu_p = 1.5 \times 10^4$ $cm^2V^{-1}s^{-1}$ for intrinsic Si and μ_e = 1.2×10^4 $cm^2V^{-1}s^{-1}$, $\mu_p = 3.5 \times 10^3$ $cm^2V^{-1}s^{-1}$ for intrinsic Ge. Using Eq. (1) and the formula for the Hall coefficient, we can also estimate what should be the Hall mobility for intrinsic Si and Ge. At room temperature, the intrinsic Si carrier densities are $n = p = n_i = 1.5 \times 10^{10}$ cm^{-3}, and the electron and hole drift mobilities are μ_e = 1500 $cm^2V^{-1}s^{-1}$ and μ_p = 450 $cm^2V^{-1}s^{-1}$, correspondingly. Thus, one can estimate the Hall mobility to be 1050 $cm^2V^{-1}s^{-1}$. Analogously, for intrinsic Ge, $n = p = n_i = 2.4 \times 10^{13}$ cm^{-3}, and the electron and hole drift mobilities are μ_e = 3900 $cm^2V^{-1}s^{-1}$, μ_p = 1900 $cm^2V^{-1}s^{-1}$. Thus, the Hall mobility for Ge is 2000 $cm^2V^{-1}s^{-1}$. The calculated Hall mobility μ_H at 77 K for intrinsic Si and Ge is 1.5×10^4 $cm^2V^{-1}s^{-1}$ and 8×10^3 $cm^2V^{-1}s^{-1}$, respectively.

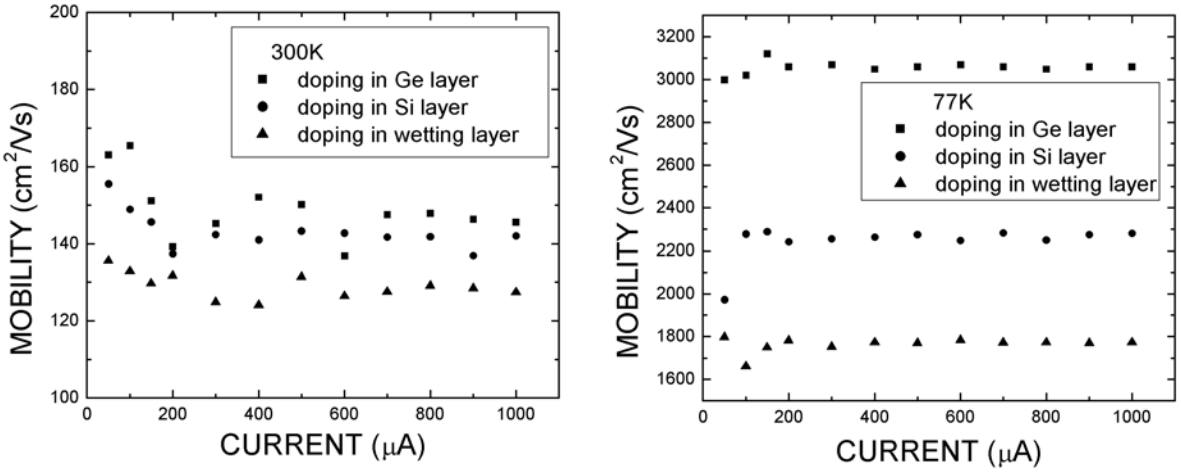

Fig.2 Hall mobility μ_H in the doped Ge/Si quantum dot superlattice at room temperature (a), and at 77 K (b).

As one can see from Table I, the average measured Hall mobility for the doped Ge/Si quantum dot superlattices is about 140 $cm^2V^{-1}s^{-1}$ in room temperature and 2.4×10^3 $cm^2V^{-1}s^{-1}$ at 77 K (averaged for three types of samples). The average value for the undoped QDS is 233.5 $cm^2V^{-1}s^{-1}$ at room temperature, and 6.80×10^3 $cm^2V^{-1}s^{-1}$ at 77 K. These values are much less than those for Si and Ge Hall mobilities. Another observation is that the Hall mobility in these QDS does not strongly depend on the location of δ-doping. The measured Hall mobilities are about a factor of two less than the drift hole mobility in intrinsic Ge. At the same time the QDS Hall mobility values are larger than

typical mobility values in the hopping conduction regime. The decrease of the Hall mobility in QDS compared to the bulk intrinsic value can be attributed to the presence of the potential barriers at the Ge/Si interface, charging effects, surface disorder, dislocation and alloy scattering, etc. Moreover, most of the band discontinuity between Ge and Si resides in the valence band thus stronger impeding the hole transport. The apparent Hall carrier concentration is larger in the doped QDS samples than that in the undoped QDS samples. The Hall mobility in the doped QDS is lower, which might be attributed to the presence of additional carrier relaxation mechanisms in these samples such as scattering on dopant atoms. A study of the dislocation line density conducted for the samples grown by the same group [J.L. Liu, J. Wan, K.L. Wang, D.P. Yu, *J. Crystal Growth*, **251**, 666 (2003).] indicates that the high-density dislocations are generated when the number of layers is larger than 25. Thus, in the investigated QDS samples the role of the dislocation lines on the carrier transport is not expected be dominant. Further research is needed in order to make definite conclusions about the contribution if any of the wetting layers on the carrier transport and mobility. The fact that the mobility is the lowest in the samples with δ-doping in the wetting layer suggests that they do contribute to the transport.

Table I. Hall mobility in Ge/Si quantum dots superlattices

QUANTUM DOT SUPERLATTICES	300 K		77 K	
	μ_H (cm^2/Vs)	N_b (cm^{-3})	μ_H (cm^2/Vs)	N_b (cm^{-3})
Ge/Si QDS (JL264 undoped N=5)	239	7.57×10^{18}	7.2×10^3	2.86×10^{18}
Ge/Si QDS (JL265 undoped N=20)	228	1.76×10^{18}	6.4×10^3	7.98×10^{17}
Ge/Si QDS (LJ017 doping in Ge layer N=5)	149	3.13×10^{19}	3.1×10^3	8.37×10^{18}
Ge/Si QDS (LJ018 doping in Si layer N=5)	143	2.89×10^{19}	2.2×10^3	6.10×10^{18}
Ge/Si QDS (LJ021 doping in wetting layer N=5)	129	3.79×10^{19}	1.8×10^3	6.51×10^{18}

As seen from Table I, the Hall mobility at 300 K is much smaller than that at 77 K, which is characteristic for the band conduction-type transport. Indeed, in conventional semiconductors, mobility increases with decreasing temperature (from 300 K to 77 K) due to reduction in phonon scattering. In the hopping transport regime, characteristic for disordered systems, the temperature dependence of the mobility is different. This regime is sometimes observed in quantum dot arrays [A.I. Yakimov, A. V. Dvurechenskiĭ, A. I. Nikiforov, and A. A. Bloshkin, *JETP Lett*., **77**, 376 (2003); A. I. Yakimov, A. V. Dvurechenskii, A. I. Nikiforov, and C. J. Adkins, *phys. stat. sol.* (b), **218**, 99 (2000).] or nanoparticle samples. Under the assumption of conventional phonon-assisted hopping transport regime the conductance in quantum dot array is described by the equation [A.I. Yakimov, A. V. Dvurechenskiĭ, A. I. Nikiforov, and A. A. Bloshkin, *JETP Lett*., **77**, 376

(2003); A. I. Yakimov, A. V. Dvurechenskii, A. I. Nikiforov, and C. J. Adkins, *phys. stat. sol.* (b), **218**, 99 (2000).] $G(T)=G_o\exp\{-(T/T_o)^x\}$, where T_o is a parameter determined by the properties of the material, and parameter $x<1$ is defined by the energy dependence of the density of states near the Fermi level. In the case when the interaction energy between electron and a hole is large compared to energy perturbation due to disorder, parameter $x=1/2$, and the conductivity is described by the Efros-Shklovskii law [A.L. Efros and B.I. Shklovskii, *J. Phys. C*, **8**, L49 (1975).]. In the hopping transport regime, the mobility is higher and, correspondingly, the resistivity is lower, at high temperature than at low temperature due to the temperature activation mechanism. Results of our measurements suggest that for given Ge/Si quantum dot superlattices the carrier transport is of the band type rather than thermally activated hopping type [M. Furlan, *Phys. Rev. B*, **57**, 14818 (1998).]. At the same time, the final conclusions about the transport mechanisms in QDS can be made only after accumulation of sufficiently more experimental data. For comparison, the low temperature (4.2 K) mobility value in conventional Si/Ge quantum well superlattices is about 1.4×10^4 $cm^2/(Vs)$ [Yu.G. Avarov, N.A. Gordilov, V.N. Neverov, G.I. Kharus, N.G. Shelushinina, O.A. Kuznetsov, L.K. Orlov, R.A. Rubtsova, and A.L. Chernov, *JETP Lett*., **59**, 245 (1994).]. Hole mobility in strained $Si_{1-x}Ge_x$ alloys for $0.17<x<0.29$ as reported in Ref. [K.B. Joelsson, Y. Fu, W.-X. Ni and G.V. Hansson, *J. Appl. Phys*., **81**, 1264 (1997).] is in the range from 49.8 cm^2/Vs to 30.3 cm^2Vs (at doping concentrations from $2x10^{18}$ to $7.5x10^{18}$ cm^{-3}), which is noticeably smaller than in QDS investigated in the present work.

In summary, we measured Hall mobility in a set of doped and undoped Ge_xSi_{1-x}/Si quantum dot superlattices. The average in-plane Hall mobility for p-type structures was determined to be 140 $cm^2V^{-1}s^{-1}$ at room temperature and 2.4×10^3 $cm^2V^{-1}s^{-1}$ at 77 K. The Hall mobility only weakly depended on the location of δ-doping. Relatively large mobility values and its temperature dependence suggest that the carrier transport is of the band conduction type rather than hopping conductivity type in these quantum dot superlattices. These results are important for proposed thermoelectric application of quantum dot superlattices.

b) Thermal conductivity of Ge quantum dot superlattices

In this research, we accomplished systematically the investigation of cross-plane thermal conductivity of Ge quantum dot superlattices.

Samples (A through G) were grown by a solid source molecular beam epitaxy (MBE) system on Si (100) substrates. The nominal growth rates were 1 and 0.2 Å/s for Si and Ge, respectively. The growth started with a 100nm Si buffer layer, followed by the quantum dot superlattice layers that are composed of bi-layers in which the Ge dot layers are separated by a 20nm Si spacer layer. The periods and nominal Ge thickness are different for various samples. To investigate structural properties of the samples, transmission electron microscopy (TEM) and atomic force microscopy (AFM) were used. Figure 3a shows a typical cross-sectional TEM image of sample C. The 10-period vertically correlated Ge quantum dot layers are evident. Fig. 3b shows an AFM image of sample C. All dots appear as domes and pyramids. The density is $4.1\times10^9 cm^{-2}$. The

average dot base and height were determined to be 14 nm and 122 nm, respectively. Here, the AFM tip effect on the dot size quantification has been calibrated by TEM and taken into account. Similar measurements have been performed on other samples as well. The structural data are summarized in Table II.

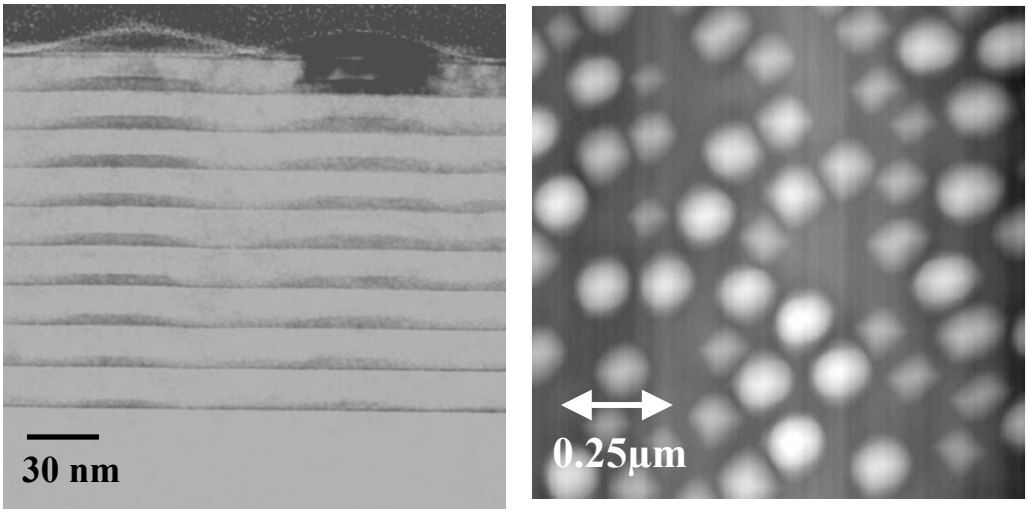

Fig.3 (a) TEM image of sample C, (b) AFM image of sample C.

Table II: Structural data of samples investigated.

Sample	Growth T (°C)	Period	Ge layer Thickness (Å)	Si layer Thickness (nm)	Dot base (nm)	Dot height (nm)	Density (cm^{-2})
A	500	10	15	20	114.7	15.1	5.9×10^{8}
B	540	10	12	20	110.4	11.9	3.6×10^{9}
C	540	10	15	20	122.0	14.0	4.1×10^{9}
D	540	10	18	20	122.2	16.0	3.5×10^{9}
E	600	22	15	20	175.5	10.2	2.6×10^{8}
F	600	22	12	20	152.4	10.0	1.4×10^{8}
G	600	25	6	20	-----	----	------

Thermal conductivity of the samples was measured by a differential 3ω method [T. Borca-Tasciuc, A. R. Kumar, and G. Chen, Rev. Sci. Inst. **72**, 2139(2001)]. The reference sample used for differential measurement is the same as the substrate used in sample growth. On each sample, a PECVD silicon nitride layer, about 100nm thick, was deposited to provide electrical insulation for the measurement. Gold 3ω heater-thermometer wires were patterned and fabricated on top of the nitride layer. The measurements were conducted inside a vacuum cryostat that operated from 80K to 300K. For each temperature point, a wide frequency range, from 300Hz to 5000Hz, is adopted in the temperature rise signal sampling. The thermal conductivity in the cross-plane direction is obtained from a fitting program, which can also be used to extract the thermal conductivities of the nitride layer and the Si substrate as a way of checking the accuracy of measurement.

Figure 4 shows the thermal conductivity versus measurement temperature for sample C and bulk Si and bulk Ge. A large reduction in the cross-plane thermal conductivity of the quantum dot sample as compared with the value of the bulk Si and Ge samples is observed. The peak value on the K-T curve shifts to a temperature as high as about 200K, compared with about 10-30 K for bulk material. This is a typical indication of the quantum size effect. Figure 5 shows the thermal conductivity as a function of measurement temperature for all the samples. For the group of samples grown at 540°C, the data above 200K shows that with the increase in Ge dot size, the thermal conductivity decreases. This trend is not obvious for the data below 200K, mainly because of the relatively small thickness of the samples grown at 540°C (10 periods). A similar trend is also observed for the group of samples grown at 600°C. For the samples with the same Ge equivalent thickness but grown at different temperatures (A, C, and E), the results show that the higher the growth temperature, the larger is the thermal conductivity. Figure 6 summarizes the room-temperature thermal conductivity as a function of the nominal Ge layer thickness. Error bars represent the fluctuations among the values from measurements at different times and for wires having different sizes. Line 1 shows that there is a slight dependence of thermal conductivity on nominal Ge thickness for the

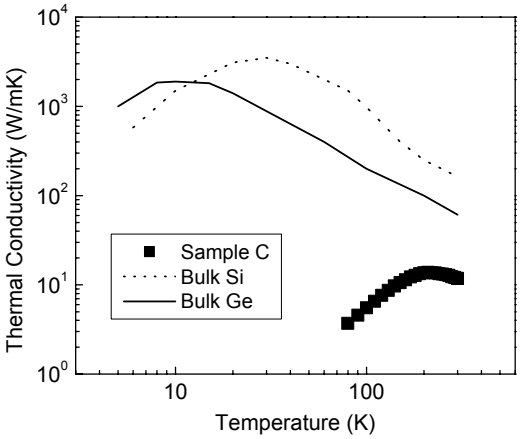

Fig.4 Thermal conductivity as a function of temperature for quantum dot sample C and bulk single-crystal Si and Ge.

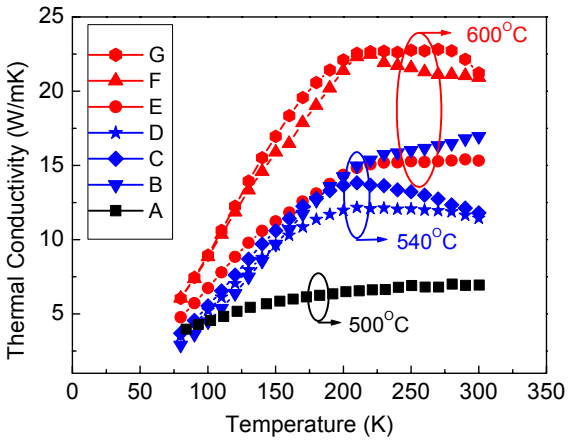

Fig.5 Thermal conductivity as a function of temperature for samples grown at different temperatures and with different Ge equivalent thicknesses.

samples grown at the same substrate temperature. Line 2, however, suggests that for the same nominal Ge layer thickness, there is a much more significant change in thermal conductivity for the samples grown at the different substrate temperatures.

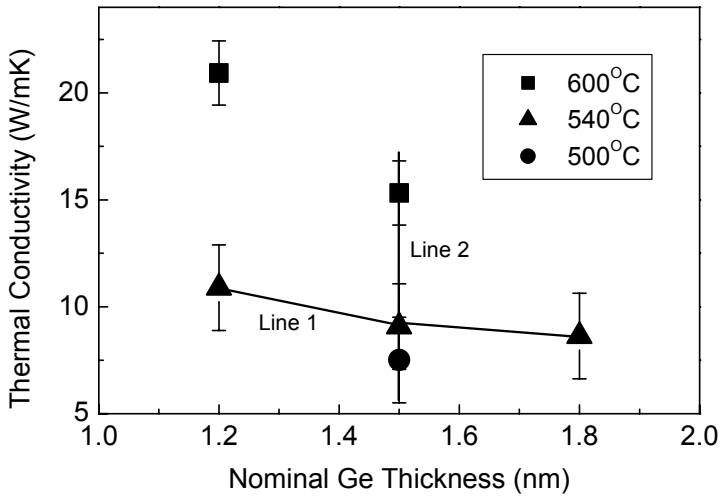

Fig.6 Room temperature thermal conductivity as a function of nominal Ge thickness.

In order to explain the above results, we realize that the expression for the lattice thermal conductivity in the relaxation-time approximation can be written as [G.P. Srivastava, *The Physics of Phonons* (Adam Hilger, New York, New York, (1990), p. 128.; P.G. Klemens, in *Solid State Physics*, edited by F. Seitz and Turnbull (Academic, New York, 1958), Vol. 7, p.1.]

$$\kappa = \frac{1}{3}\sum_i \int dk v_{g_i}^2(k)\tau_{C_i}(k)S_i(k) \qquad \text{(b1)}$$

where i denotes a particular phonon polarization branch, $v_{g\,i}$ is the phonon group velocity associated with the ith branch, τ_C is the combined relaxation time, $S_i(k)dk$ is the contribution to the specific heat from modes of the polarization branch i in the phonon wave vector interval of kdk. The combined relaxation time τ_C includes all relaxation rates corresponding to the different scattering processes, which do not conserve crystal momentum

$$\frac{1}{\tau_C} = \sum \frac{1}{\tau} = \frac{1}{\tau_M} + \frac{1}{\tau_B} + \frac{1}{\tau_U} + \frac{1}{\tau_D} \qquad \text{(b2)}$$

Here, $1/\tau_U$ is the three-phonon Umklapp processes, $1/\tau_M$ is the phonon-point defect scattering (isotopes, impurities, etc.), $1/\tau_B$ in the phonon-boundary scattering, and $1/\tau_D$ is the phonon scattering by the quantum dots [A. Khitun, A. Balandin, J.L. Liu, and K.L. Wang, J. Appl. Phys. **88**, 696 (2000).]. Eq. (b2) includes the phonon relaxation processes, which are dominant in Si, Ge, and Si_xGe_{1-x} structures. The expressions for phonon relaxation rates $1/\tau_U$, $1/\tau_M$, and $1/\tau_B$ were derived by Klemens in Ref. [P.G. Klemens, in *Solid State Physics*, edited by F. Seitz and Turnbull (Academic, New York, 1958), Vol. 7, p.1.]. The new term $1/\tau_D$ is related to the phonon scattering on quantum

dots. The most general expression for the phonon scattering rate on quantum dots can be written as

$$\frac{1}{\tau_D} = \frac{v_g \sigma_V}{V} \tag{b3}$$

where σ_V is the total cross section of the dot ensemble of volume V. Here, we treat all dots as equal spheres with radius a on a plane, which is perpendicular to the growth direction. To describe the phonon transport in quantum dot superlattices, we use the continuum model approximation and an assumption that the thermal phonon wave can be represented by a sum of plane waves [A. Khitun, A. Balandin, J.L. Liu, and K.L. Wang, J. Appl. Phys. **88**, 696 (2000).]. Thus, the expression for the scattering cross section σ of a single quantum dot becomes [P.M. Morse and H. Feshbach, Methods of Theoretical Physics, (McGraw-Hill Book Company, Inc., New York, 1953), Part II, pp. 418-430 (1953).]

$$\sigma = \frac{\pi}{k^2} \sum_{m=0}^{\infty} (2m+1) \left| 1 + R_m \right|^2 . \tag{b4}$$

In the above equation, R_m is a reflection coefficient

$$R_m = \frac{h'^*_m(ka) + i\beta h^*_m(ka)}{h'_m(ka) + i\beta h_m(ka)} \tag{b5}$$

where $\frac{c}{{}_e c_e} \left\lfloor \frac{{}'_m(\ a)}{{}_m(\ {}_e a)} \right\rceil$, ρ is the density, c is the sound velocity, the subscript e denotes tl dot material, $h_m(ka) = j_m(ka) + iy_m(ka)$, j and y are the spherical Bessel functions of the first and second kinds, respectively, and h^*_m is the complex conjugate. Because of Si/Ge interdiffusion, the quantum dots are not pure Ge. Average Ge compositions were obtained by Raman scattering for these quantum dot samples [J. L. Liu, J. Wan, Z. M. Jiang, A. Khitun, K. L. Wang and D. P. Yu, J. Appl. Phys. **92**, 6804(2002).]. The particular density and sound velocity inside a dot are modified by the Ge composition in the quantum dot. We use an approximate formula $\rho_e = \rho_{Ge} \cdot x + (1-x)\rho_{Si}$ and $c_e = c_{Ge} \cdot x + (1-x)c_{Si}$, where x is the Ge composition.

In order to find final σ_V, we have to sum the contributions from all scattered waves from all the dots in the unit volume V taking into account dot ordering in the layers. At some arbitrary point, the reflected amplitude S normalized to the amplitude of the incident plane wave is given as

$$S = \frac{\left| F(\vartheta) \right|^2}{r^2} \sum_{n=1}^{N} e^{(iur_n)} \tag{b6}$$

where the scattering function $F(\vartheta)$ is:

$$F(\vartheta) = \frac{i}{2k} \sum_{n}^{\infty} (2n+1)(1+R_n) P_n(\cos\vartheta) \tag{b7}$$

and $P_n(\cos\vartheta)$ are Legendre polynomials, where $u=k_0-k$, k and k_0 are the wave vectors of the plane and scattered waves. The sum in Eq. (b6) can be split into two terms:

$$\sum_{n=1}^{N} e^{(iur_n)} = \left[N + \sum_{n \neq m}^{N} e^{(iur_{mn})} \right] \tag{b8}$$

The first term on the right hand side of Eq. (b8) is the number of dots in volume V and represents the scattering of phonons from quantum dots when they act as independent scattering centers. We refer to this as the *incoherent* scattering term. The second term on the right hand side of the Eq. (b8) represents the cooperative scattering action of the quantum dots. We refer this to the *coherent* scattering term, in analogy with the terminology adopted in acoustics [P.M. Morse and H. Feshbach, Methods of Theoretical Physics, (McGraw-Hill Book Company, Inc., New York, 1953), Part II, pp. 418-430 (1953).]. An appearance of the coherent scattering in the cross plane direction is caused by the dot ordering in the layers.

In general, the problem of finding the total cross section, σ_V, can be done only numerically. Averaging of the scattering effects produced by a single quantum dot layer can result in a significant simplification of the calculation procedure. The re-scattering from all scatters in a given zone will be, on average, equal in magnitude but opposite in sign from the contribution of the pre-sending zone. Following this stationary phase approach only scatters within the first Fresnel zone contribute to the transmitted wave field. By definition these scatters radiate in phase with the background wave field, which means that the precise location of the scatter is of minor importance. The discrete distribution of the scatters can be replaced by a smooth scatter density, ν. We use the result obtained in Ref. [J. Groenenboom and R. Snieder, J.Acoustic. Soc. Am. **98** (6), 3482(1995).] for the transmission coefficient of a single layer :

$$T = \left(1 - i\frac{\nu_s}{2k} f(0)\right) \qquad \text{(b9)}$$

where ν_s is the sheet dot density in the layer. The weak scattering density limit is defined by the requirement $|\nu f(0)/k^2| << 1$, which is well satisfied due to the finite acoustic mismatch between Si and Ge up to 10^{10} dots/cm^2 density.

The effects of scattering on quantum dots affect other relaxations times via phonon dispersion modification. In the cross-plane direction the increased phonon scattering modifies the phonon dispersion in such a way that acoustic phonons travel with a group velocity different from the one in bulk. The procedure calculating the cross-plane thermal conductivity consists of a number of steps. First, we calculate the single dot scattering function (Eqs. (b5-b7)). Then, we calculate the total cross section for the quantum dot superlattice taking into account dot ordering in space (Eqs. (b6-b9)). Next, we calculate the set of relaxation times using Eq. (b2), taking into account dispersion modification. Finally, we obtain the lattice thermal conductivity using Eq.(b1).

The total scattering on quantum dots in the considered temperature range exceeds those caused by phonons and isotopes. This results in a significant cross-plane lattice conductivity decrease as well as modification of the thermal conductivity temperature dependence. In Figure 7, we show a plot of thermal conductivity versus temperature for SiGe quantum dot surperlattice samples A, B and F. It is clear that the calculated temperature dependence of thermal conductivity for all samples are in good agreement with the experimental data. The results of numerical simulation show the same shift of the superlattice K-T curve peak position in comparison with the curve from bulk materials in Fig.3. The good agreement between the calculated and experimental data validates our approach based on the continuum model approximation and the assumption

that the thermal phonon wave can be represented by a sum of plane waves affected by the scattering on acoustically mismatched obstacles.

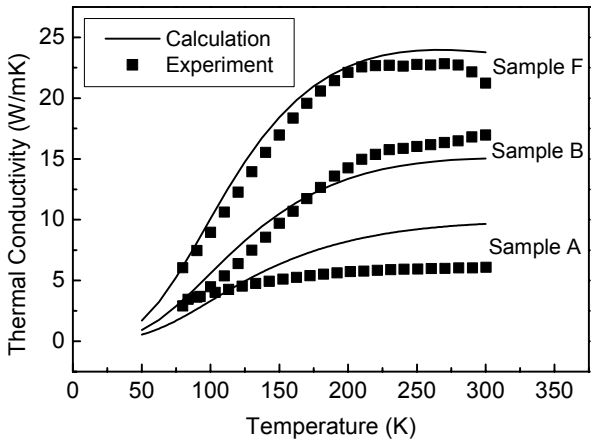

Fig.7 Comparison of experimental and calculated thermal conductivity as a function of measurement temperature for three samples.

In summary, we achieved the temperature dependent thermal conductivity of different Ge quantum dot superlattices and a theoretical explanation for the obtained results. It is found that the thermal conductivity of the Ge quantum dot superlattices is significantly reduced compared with the bulk values of Si and Ge.